Facial nerve stimulation in a post-meningitic cochlear implant user: using computational modelling as a tool to probe mechanisms and progression of complications on a case-by-case basis

Werner Badenhorst*, Tania Hanekom, Liezl Gross and Johan J. Hanekom

Bioengineering, Department of Electrical, Electronic and Computer Engineering, University of Pretoria, Pretoria, South Africa

*Corresponding author

Werner Badenhorst

Office: +27 12 420 2587

Email: werner.badenhorst@up.ac.za

Website: www.up.ac.za/bioengineering

Word count:

6321 (including tables, references, figure captions; excluding title page, abstract page, reference list).

Abstract

Facial nerve stimulation (FNS) is a side-effect of cochlear implantation that can result in severe discomfort for the user and essentially limits the optimal use of the implant. In recent years, research in the field of three-dimensional cochlear implant modelling has led to the progression from generic models to user-specific models with one of the intentions to develop model-based diagnostic tools. The objective of this study is to investigate the mechanisms that underlie the manifestation of FNS in the post-meningitic cochleae of a specific CI user through computational modelling. Bilateral models (right and left) were created using a method previously developed for the construction of a three-dimensional user-specific volume conduction model of the cochlea and was expanded to include the facial nerve geometry. Reduced temporal bone density based on bone densitometry, cochlear duct ossification and degenerate auditory neural fibres were incorporated into a comprehensive FNS model. Auditory and facial nerve thresholds were predicted with the models showing good correspondence to perceptual thresholds and the user's FNS experience. Ossified cochlear ducts appear to aggravate the increase in thresholds caused by the otic capsule's decreased resistivity. This translational case study demonstrates the application of computational modelling as a clinical instrument in the assessment and management of complications with CI implantation.

Keywords: 3D cochlear model; bone densitometry; user-specific CI model; compound model

Introduction

Cochlear implantation is a conventional and safe rehabilitation method of profoundly deaf people and has improved the quality of life of many individuals. However, some users suffer post-implantation complications (Farinetti et al., 2014; Postelmans et al., 2007) as the biological conditions near the electrodes affect the functioning of the implant (Pfingst et al., 2011). One such complication is facial nerve stimulation (FNS) (Ahn et al., 2009; Akst & Weber, 2005; Berrettini et al., 2011; Bigelow et al., 1998). FNS can result in considerable discomfort for users and effectively limits the optimal use of the CI (Seyyedi et al., 2013). FNS occurs when the electrical current from the electrode spreads outside the cochlea, thereby stimulating nearby nerves such as the facial nerve (FN) (Ahn et al., 2009; Bigelow et al., 1998; Niparko et al., 1991).

Symptoms of FNS can range from awareness of tingling in the face to severe facial spasms that may have an immediate onset at device switch-on or a delayed onset after a period of use (Ahn et al., 2009; Berrettini et al., 2011; Seyyedi et al., 2013). CI-related FNS has been widely reported in the literature and several causes, such as insertion trauma, cochlear malformation, cochlear ossifications and otosclerosis, have been identified (Ahn et al., 2009; Battmer et al., 2006; Berrettini et al., 2011; Cushing et al., 2006; Kruschinski et al., 2003; Seyyedi et al., 2013).

Another challenge for CI rehabilitation occurs in cases of sensorineural hearing loss (SNHL) caused by meningitis infection and the subsequent ossification of the cochlear ducts (Axon et al., 1998; Bille & Ovesen, 2014; Caye-Thomasen et al., 2012) obstructing the insertion of the electrode array. This damaging process usually starts within the basal turn of the scala tympani (ST), causing more severe loss in higher frequencies(Du et al., 2006; Eshraghi et al., 2004; Johnson et al., 1995). Some studies have found that post-meningitic CI users, despite some having a full insertion, often

battle with poorer speech performance compared to non-meningitic users as even mild ossification can influence performance with a CI (Rauch et al., 1997).

In recent years, the application of user-specific three-dimensional (3D) CI models has been translated from the research domain where these models are used to understand the physiological and scientific basis for the functioning of CIs, to the clinical domain where they are applied as a diagnostic tool to support the management of CI performance for individual users. Model-based diagnostic (MBD) tools could allow non-invasive, quantitative analysis of problems that may arise at the biophysical interface between the implant and the cochlea (Hanekom & Hanekom, 2016; T.K. Malherbe et al., 2013; T. K. Malherbe et al., 2015). The MBD tool used in the present study consists of a 3D volume conduction (VC) model used in conjunction with a computational neural model. The resulting compound model is used to predict the effect of the spread of stimulation current within the cochlea on neural excitation characteristics (Hanekom, 2005). A study by Frijns et al. (2009) sucessfullly made use of 3D VC modelling to explore FNS in an otosclerotic ear with a CI. They employed a generic model of the human cochlea and the FN to examine the effect of temporal bone conductivity and electrode placement on FNS.

The objective of this case study is to investigate the mechanisms that underlie the manifestation of FNS in a specific user's post-meningitic cochleae through the use of computational modelling. User-specific 3D VC models were created for the left and right cochleae and FNs for an 18-year old female suffering from SNHL resulting from meningitis and who started experiencing FNS ten years post-CI implantation. Bone densitometry was used to estimate the reduced temporal bone resistivity. Additional post-meningitic factors included in the model were ossified cochlear ducts and degenerate ANFs. Subsequent predicted ANF and FN THRs were used to investigate

the effect of varying temporal bone resistivity, the correspondence with perceptual THRs, the predicted likelihood of FNS compared to the user's experience and the relationship between electrode distance from the FN and its risk of causing FNS. Results suggest that an MBD tool may facilitate the analysis of FNS for a specific user which may, in turn, inform a protocol to deal with the complication.

Methodology

CI user history

Ethical clearance from the University's ethics committee as well as informed consent from the CI user were obtained to conduct this study.

The participant in this study received her first implant (Med-El C40+ Standard Electrode array) in the right ear at age four years and four months (Apr. 2002), two years and seven months post-meningitis infection. Three years later the left cochlea was implanted with a Med-El Pulsar ci100 short array because of severe ossification of the scalae. Another three years later, she started to experience acute headaches and pain on the left side that worsened over time to the point where she refused to wear the left processor (Jan. 2010) and eventually had it explanted because of fluid draining over the implant (Aug. 2012). A dummy electrode was inserted to facilitate future re-implantation despite further ossification. At the end of 2013, with only the original right processor in use, facial nerve stimulation (FNS), mostly eye twitches, was noted for the first time and the user complained that sounds were becoming too soft. A new map was programmed that initially performed well and did not cause eye twitching, but over time, increased stimulation levels triggered the eye twitch again. In October 2014 the left ear was re-implanted (Med-El Compressed Array and SONATAti100 processor), but ossification allowed only 7 of 12 electrode contacts to be inserted.

Shortly after activation of the new implant, FNS was noted on the left side as well. The FNS progressed on both sides and in mid-2015 (age 17) the user's ENT decided to try Botox (Botulinum Toxin) treatment as a possible short-term solution to the FNS, as this method has been shown to be effective in the elimination or reduction of FN hypersensitivity (Langman et al., 1995). Although the treatment inhibited the FNS, the user still occasionally perceived “invisible jumps” of the facial muscles and also had little or no facial expression which had negative social implications. This treatment was therefore not considered as a long-term solution.

Applying the MBD tool to assess the specific CI user's FNS

Basic user-specific CI model

The basic user-specific CI model at the core of the MBD instrument consists of a finite element volume conduction (FEVC) model of a cochlea that is integrated with an ANF model. The FEVC model is a computational description of the anatomy and electrical properties of a cochlea and the dimensions and electrical properties of a specific electrode array inserted into the cochlea. It allows calculation of the spread of current throughout the modelled volume as a result of intracochlear stimulation. The ANF model is a computational description of the morphology and electrophysiology of nerve fibres under electrical stimulation. The ANF model allows calculation of a neural response to the current distribution from a specific stimulus as predicted by the FEVC model.

FEVC models were created for the user's left and right cochleae using the method presented in our previous work (Badenhorst et al., 2017; T.K. Malherbe et al., 2013; 2015, 2016). A full insertion of twelve active electrodes (Med-El Classic Series

Standard) was modelled for the right cochlea, and a partial insertion of seven active electrodes was modelled for the left cochlea (Classic Series Compressed).

Each cochlea was encapsulated by a spherical otic capsule modelled as homogeneous temporal bone. The left and right otic capsules were subsequently positioned in a generic FEVC head model, scaled to the user's head dimensions.

Neural excitation was predicted using the Hodgkin-Huxley-based human compartmental ANF neural model of Rattay et al. (2001) as implemented in Badenhorst et al. (2017). Single ANFs were spaced at 5° intervals along the angular length of the cochlea following a radial pattern from the modiolus into the spiral lamina.

Adding the FN to the basic model

The construction of the FEVC model of the FN was based on the dimensions from the three temporal sections of the FN, i.e. the labyrinthine, tympanic and mastoid segments stretching from the internal acoustic meatus to the stylomastoid foramen (Maru et al., 2010). The path and dimensions of the three segments were determined using the method by Shin et al. (2014) based on the visible FN (fallopian) channel on the CT scans. The widths (diameters) of the labyrinthine (WL) and tympanic segments (WT), the length of the labyrinthine segment (LLS) and the angle between the labyrinthine and tympanic segments (ALT) were measured from the axial CT view shown in Figure 1a. From the oblique coronal view (Figure 1b), the length of the mastoid segment (LMS) and its width (WM), the length of the tympanic segment (LTS) and the angle between the tympanic and mastoid segments (ATM) were measured. Results were validated against measurements reported in the literature (Fatterpekar et al., 2006; Phillips & Bubash, 2002; Şentürk et al., 2009; Shin et al., 2014).

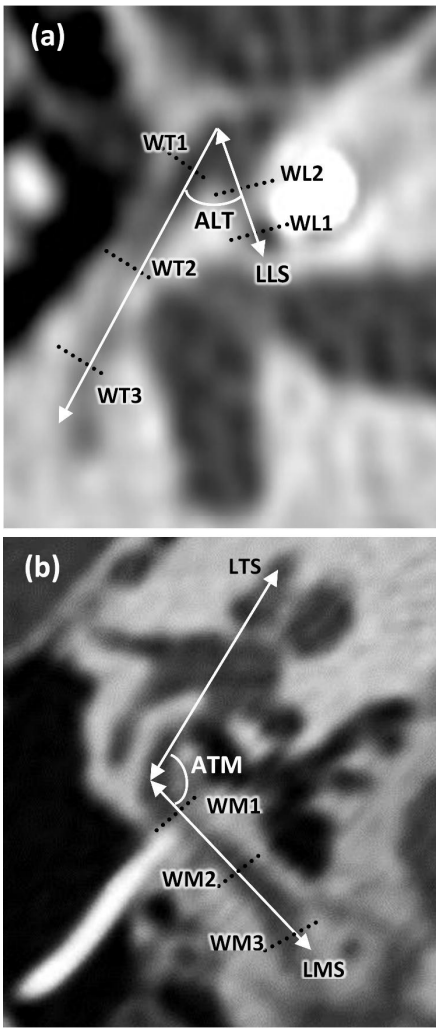

Figure 1. CT-based measurements of the facial nerve landmarks for one FN. (a) Axial view showing the angle between the labyrinthine and tympanic (ALT) segments, the widths (diameters) of the labyrinthine and tympanic segments (WL1, WL2, WT1 – WT3) as well as the length of the labyrinthine segment (LLS). (b) Oblique coronal view showing in the angle between the tympanic- and mastoid segments (ATM), the widths of the mastoid segment (WM1 – WM3) as well as the lengths of the tympanic- and mastoid segments (LTS, LMS).

The angular position of the geniculate ganglion was determined in relation to the origin of the cochlea as defined by the cochlear view (Verbist et al., 2010). Once the orientation and location of the FN was determined relative to the cochlea, its geometric coordinates were calculated and imported in the basic FEVC CI models (Figures 2 and

3). As the resistivity of the FN is unknown, the resistivity of the spiral ganglion (300 Ω.cm) was used.

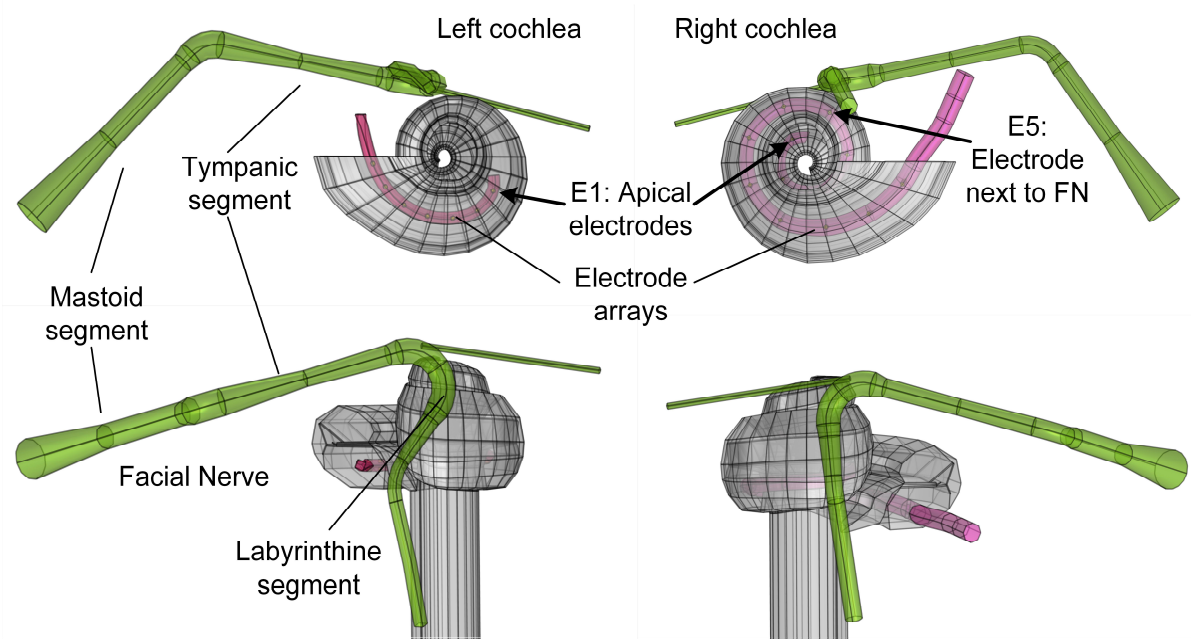

Figure 2. The semi-transparent inferior and lateral views of the left and right cochleae and FN FEVC COMSOL models show the relative location of the FN, cochlea and electrode arrays. The location of the most apical electrode contacts, E1, for the left and right arrays and also E5, which is the electrode in closest proximity to the FN for the right cochlea, are indicated.

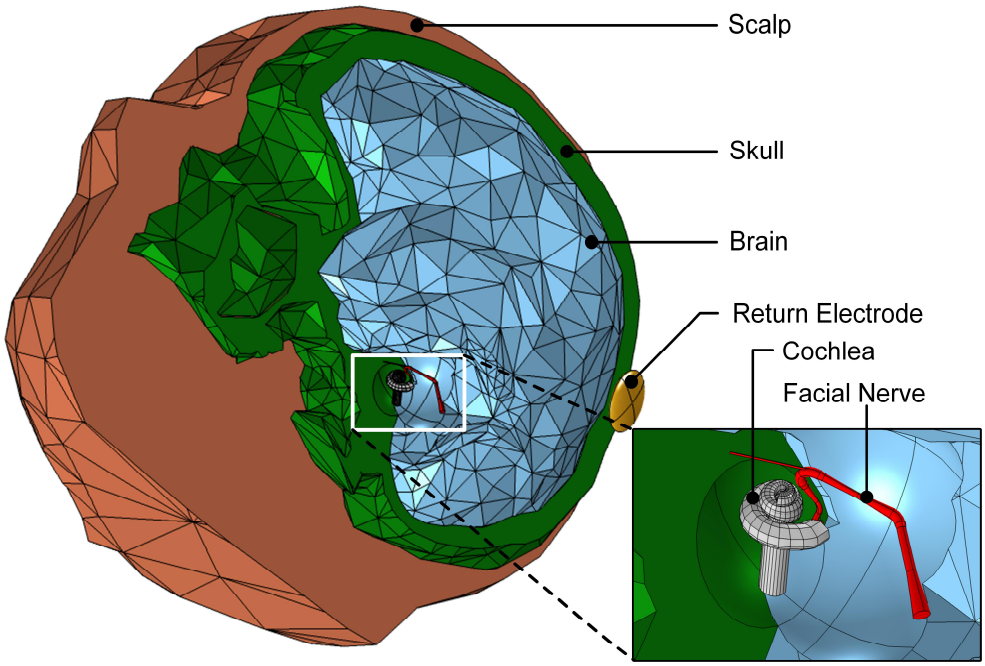

Figure 3. The complete FEVC model image shows the relative location of the scaled, generic head, the user-specific left-hand cochlea and the facial nerve.

Several assumptions were made to model FN excitation. (1) Only the motor root of the FN innervating the facial muscles was considered since the focus was on FNS resulting from CI use. (2) The segment of the motor root of the FN closest to the cochlea was modelled as a bundle of axons since somas of motor fibres of all cranial nerves are located in the respective brainstem nuclei (Shin et al., 2014). (3) Only one fibre on the perimeter of the FN closest to the cochlea was selected to determine FN thresholds since this location represents a worst-case FNS scenario. (4) Since very little about the morphology and electrophysiology of the FN is available in the literature, the FN fibre was modelled using the Rattay et al. (2001) compartmental neural model. A fibre diameter of 8 µm was chosen from the FN fibre diameter range of 4 to 8 µm reported by Thurner et al. (1993) since fibre threshold decreases as the diameter increases (Rattay et al., 2001). This choice will produce an indication of the lowest FNS threshold that may be expected and thus maintain the worst-case scenario for FNS. The internodal distances of the fibres were arbitrarily set at 500 µm as in Rattay's central axon model as no value could be found in the literature. A study by Frijns et al. (2009) used a 4 µm diameter that would predict higher FNS thresholds, and a 400 µm internodal distance.

Applying the MBD tool to the FNS case

Model validation

Validation of the MBD tool is required first to assess the model's ability to predict measured, perceptual results and second to serve as a benchmark or reference for diagnostic investigations. Model outcomes in the form of predicted, single fibre thresholds, were compared to the user's map parameters (threshold and most

comfortable loudness (MCL). Predicted thresholds are known to be higher than actual measured, perceptual thresholds making it difficult to compare thresholds and to estimate MCL levels (Kalkman et al., 2016). (Briaire & Frijns, 2006) used a predicted 1 mm activation region on the neural excitation profiles (NEPs) as an equivalent for perceptual ANF threshold and a predicted 4 mm activation region for MCL. However, applying this principle was not successful as the user's NEPs were found to be relatively "flat" resulting in dynamic ranges of only 2 to 3 dB which was not comparable with measured perceptual data. As will be seen in the results, predicted ANF threshold profiles approached the perceptual thresholds and it was thus decided to directly compare these two measures and to use the Med-EL convention that threshold is set at 10% of MCL, i.e. MCL is 10×threshold or threshold + 20 dB.

Monopolar, biphasic, cathodic-first stimuli with channel (electrode) specific pulse widths, according to the user's map, were used in all simulations to predict ANF and FNF excitation thresholds. All stimulus intensities are stated in dB re 1 μA. For the right ear, a map from 2013 when FNS was first observed, was used. For the left ear, a map from 2014 after the activation of the new electrode, was used. Unfortunately, no maps or CT scans prior to 2011, when no complications were experienced by the user, were available. Both maps are pre-Botox treatment as treatment affects threshold values.

Reference model

A "healthy" reference model was created for both the left and right cochleae with normal tissue properties and intact ANFs. The two healthy or reference models were then altered to model different facets of the user's post-meningitic cochlear environment with which to investigate the causes of the FNS.

Diagnostic investigations

Three phenomena related to either FNS or meningitis were modelled namely (i) the health of the ANFs, (ii) ossification of the cochlear ducts, and (iii) a change in temporal bone density.

ANF health. Ossification in the cochlear ducts causes segmental loss of the spiral ganglion cells and also results in degenerate fibres (Klein et al., 2008; Rotteveel et al., 2004) that affects the efficacy of the CI (Pfingst et al., 2011; Pfingst et al., 2015). Segmental loss of the SG was not modelled since it is difficult to attribute hearing loss to either spiral ganglion loss or degeneration of fibres in a live CI user. The model, therefore, implements a one-dimensional neural array along the angular length of the cochlea instead of a population distribution and all hearing loss was assumed to originate from degeneration of the peripheral processes. To model the effect of degenerate fibres, all dendrites were terminated at the 5^{th} node of Ranvier (Badenhorst et al., 2017) thus leaving 14% of the dendrite along with the pre-somatic region and soma intact. This implementation agrees with reports that degeneration of the ANF begins at the dendrite and progresses toward the soma (Felder et al., 1997; J. B. Nadol, 1990) and that most somas survive (J. B. Nadol, Jr. et al., 1989).

Ossification of cochlear ducts. The electrical resistivity of the bony structures in and around the cochlea (otic capsule) affects potential distributions predicted by VC models of the electrically stimulated cochlea thereby affecting predicted neural thresholds (T. K. Malherbe et al., 2015). Meningitis often results in partial to full ossification of the fluid-filled cochlear ducts thus significantly increasing its resistivity (Durisin et al., 2010; Tinling et al., 2004). A decrease in the existing bone density (or resistivity) in

and around the cochlea is also possible, as is the case in otosclerosis (Marshall et al., 2005). A decrease in the resistivity has been shown to be a likely cause of FNS in practice (Ahn et al., 2009; Kelsall et al., 1997) and modelling (Frijns et al., 2009).

Sites of ossification cannot be determined in vivo or readily from CT scans because of electrode artefacts, and hence the sites were assumed based on literature (Bille & Ovesen, 2014; Caye-Thomasen et al., 2012; Du et al., 2006; Tinling et al., 2004) and the user's ENT reports. The user's medical records and CT scans showed the left cochlea to be almost completely obliterated, resulting in a shallow CI insertion. The left cochlea's scalae were therefore modelled as completely ossified with a resistivity of 650 Ω.cm (fibrous or cancellous bone (Saha & Williams, 1989)) compared to normal perilymph at 69 Ω.cm. The right cochlea had a deep insertion with the possibility of some ossification in the ST. The right cochlea was thus modelled with a section of the basal-to-middle turn of the ST filled with cancellous bone tissue (ρ = 650 Ω.cm) as illustrated in Figure 4.

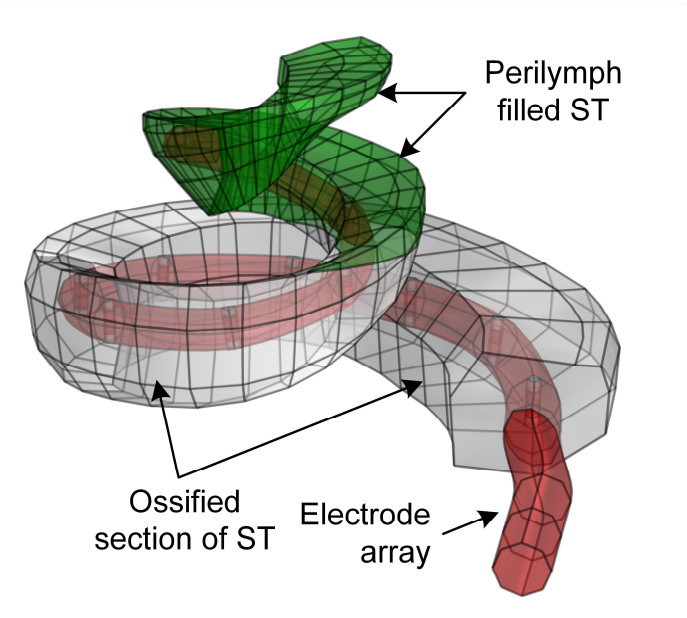

Figure 4. The FEVC model shows the basal-to-middel turn of the right cochlea's scala tympani from Figure 2 partially ossified with cancellous bone having a resistivity of 650 Ω.cm. The rest of the ST is remains filled with perilymph.

Changes in temporal bone density. To investigate how changes in bone density and hence resistivity contribute to the user's FNS symptoms and CI performance, bone densitometry was used to measure the user's temporal bone density (in Hounsfield units, HU) as an indirect, non-invasive gauge of bone resistivity. The bone densitometry method used and specific regions measured were based on four studies (Grayeli et al., 2004; Kawase et al., 2006; Kutlar et al., 2014; Marshall et al., 2005; Saha & Williams, 1989). These studies all determined bone density in otosclerotic users together with a control group of normal, healthy ears. The measurements were subsequently used in the present study as a benchmark against which to compare the density for the case of meningitis. The five regions measured are the 1) posterior semi-circular canal (PSCC), 2) fissula ante fenestrum (FAF), 3) cochlear apex, 4) precochlear region and 5) anterior margin of IAC.

For the present study, three sets of CT images taken over 18 months were used to measure the bone density for both ears at the five regions identified using INFINITT Healthcare CDViewer (medical image viewing software). Figure 5f shows the CT image passing through the oval window with the marked anatomical regions for one of the three sets.

Although there is no evidence in literature of a direct correlation between bone density and resistivity, it is known that less dense bone, such as fibrous or cancellous bone, has a lower resistivity (650 Ω.cm) (Saha & Williams, 1989) compared to normal, compact bone (Balmer et al., 2018). For the purposes of this study, any change in bone *density* will thus be interpreted as and translated to a change in bone *resistivity*. Based on the study by T. K. Malherbe et al. (2015), a bone resistivity of 6500 Ω.cm was used for normal, compact bone.

Results

Constructing the post-meningitic FNS model

Post-meningitic or FNS models that assumed degenerate ANFs and full and partial ossification of the scalae for the left and right cochleae respectively, were used to derive a suitable value for temporal bone resistivity.

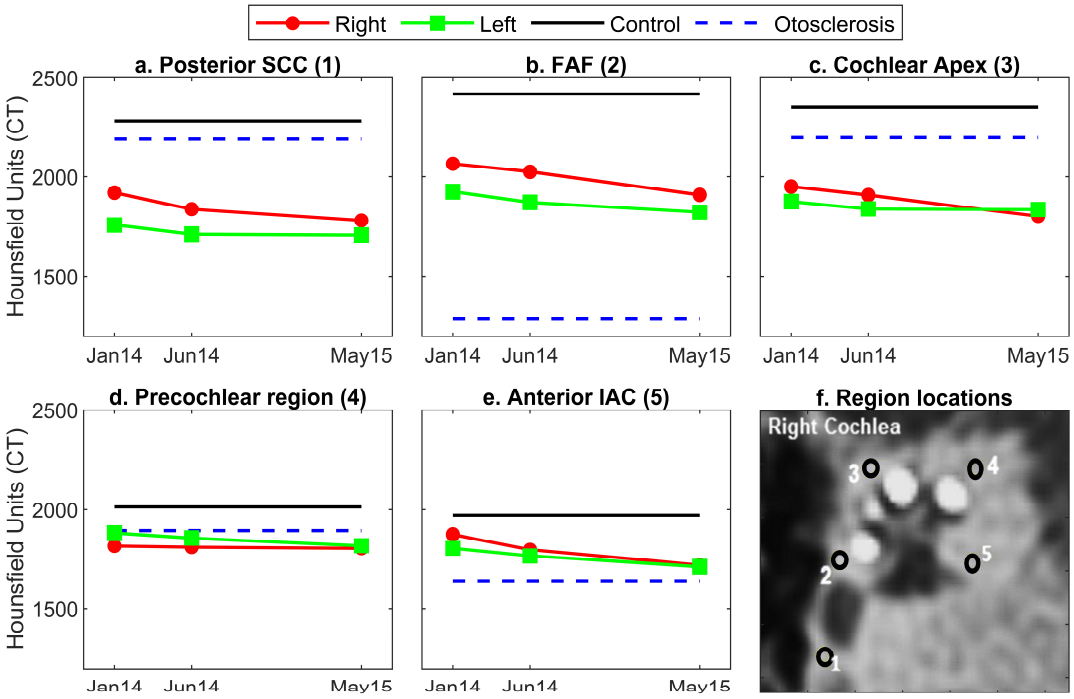

Figure 5. (a) – (e) Hounsfield units for each of the five regions for the left and right ears are compared to that of a healthy control group and an otosclerosis group. Both ears show a decrease in density over time and three regions (1, 3, 4) have lower densities than the otosclerosis group. (f) The five regions within the user's otic capsules where the bone density was measured: 1) posterior semi-circular cans (PSCC), 2) fissula ante fenestrum (FAF), 3) cochlear apex, 4) precochlear region and 5) anterior margin of IAC.

Assessment of temporal bone resistivity

The three sets of bone density measurements for each of the five regions within the otic capsule of both ears are compared to those of the average otosclerosis and control

groups in Figure 5a to e. As expected for the case of meningitis, the bone density of the user is lower than the density of the healthy cochleae of the control group. Noteworthy, however, is that the bone density, or resistivity, of both ears is lower compared to the otosclerosis group in three of the regions (PSCC, apex and pre-cochlear region) suggesting higher susceptibility to FNS compared to the otosclerosis group.

Table 1 summarizes the decrease in bone density for both cochleae over the 18 month period. An almost uniform 8% decrease in density is observed for the right ear. If the results for this ear are extrapolated to the time of reported FNS onset (Nov 2013), an overall decrease in bone density of more than 10% could be possible. The left ear shows a smaller percentage decrease in bone density which might partially be ascribed to the fact that the left ear is already fully ossified whilst the right ear is thought to be only partially ossified as discussed earlier. These results support the inclusion of a lowered temporal bone density in the user's FEVC models.

Table 1. Percentage decrease in temporal bone density in the five regions within the otic capsule over an 18 month period.

Region	% Decrease	
	Left	Right
1. PSCC	3	8
2. FAF	6	8
3. Cochlear Apex	2	8
4. Precochlear region	4	1
5. Anterior margin of IAC	5	8

Effect of temporal bone resistivity on predicted neural thresholds

To confirm the relationship between bone resistivity and neural thresholds, and provide a basis for comparison with the findings presented by Frijns et al. (2009), the effect of

temporal bone resistivity on AN and FN thresholds was investigated at values 20% and 60% lower (5200 and 2600 Ω.cm) and higher (7800 and 10400 Ω.cm) than normal, compact bone (6500 Ω.cm).

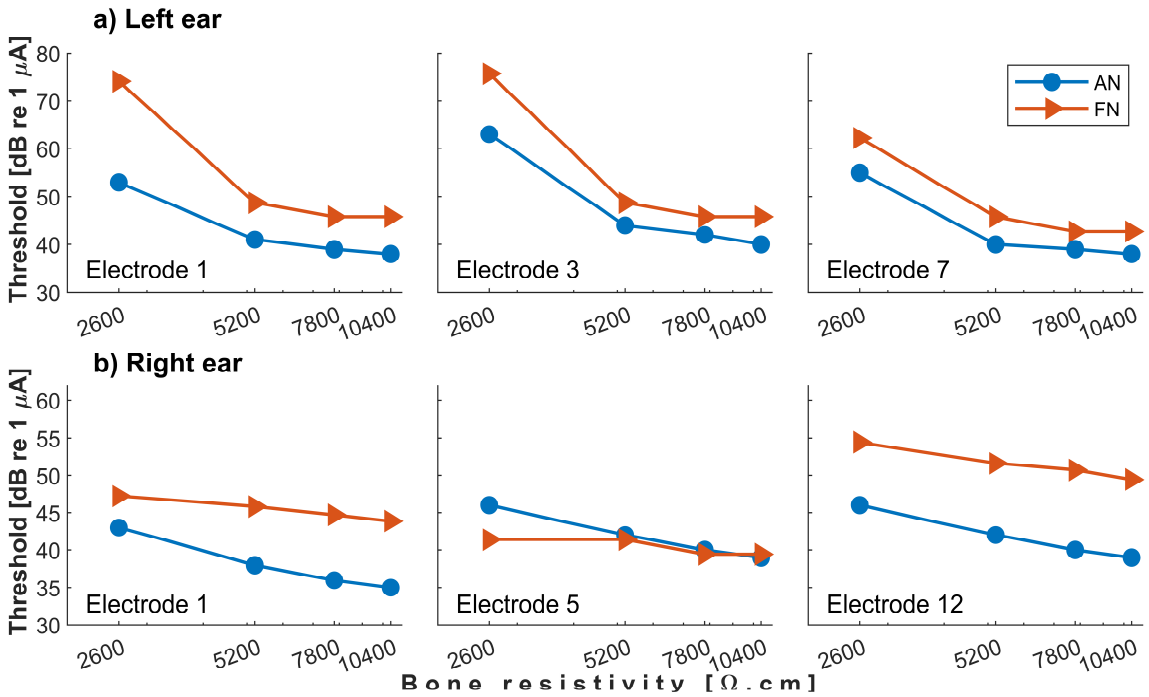

Figure 6. FNF and degenerate ANF thresholds as a function of otic capsule bone resistivity. a) Left ear shows predicted thresholds for electrodes E1 (150˚ from the round window), E3 (95˚) and E7 (5˚). Thresholds show a sharp increase below 5200 Ω.cm. E3 and E7 have threshold differences of less than 5 dB, suggesting a risk for FNS. Both ST and SV are mildly ossified with a resistivity of 650 Ω.cm. b) Right ear shows predicted thresholds electrodes E1(apical), E5 (nearest to FN) and E12 (base). The FN threshold of E5 is slightly lower than that of the ANF, suggesting a high probability of FNS. E1 and E12 pose a lower risk of FNS compared to E5 with FN thresholds more than 10 dB higher than the ANF thresholds at the majority of resistivities. Only the ST is partially and mildly ossified with a resistivity of 650 Ω.cm.

A comparison of the predicted ANF and FN thresholds at the four different temporal bone resistivities are shown in Figure 6a for the *left* ear for three electrodes. Both ANF and FN thresholds show a steep *increase* as the resistivity decreases below 5200 Ω.cm compared to a slight *decrease* above 5200 Ω.cm. For E3 and E7 the FN threshold is only approximately 5 dB higher than the ANF's suggesting a possible

increased risk for FNS. A similar comparison is shown for the *right* ear in Figure 6b. The most significant observation is E5's FN threshold being slightly lower than the ANF's, thereby suggesting a risk of FNS at low resistivities. The apical and basal electrodes present a lower risk of FNS having threshold differences of 10 to 20 dB at most resistivity values. In contrast to the left cochlea, the thresholds do not drastically increase at the lower resistivities.

Healthy reference models of the left and right ear

Predicted ANF threshold and MCL levels as well as the FN thresholds for each electrode of the healthy *left* ear were used as reference and compared to measured, perceptual user data in Figure 7a. As expected from literature, predicted thresholds are higher than the measured perceptual thresholds (Kalkman et al., 2016; T. K. Malherbe et al., 2016). Modelled and programmed with the user's map, the difference between the predicted and user's perceptual ANF threshold and MCL levels increase and diverge from approximately 10 to 18 dB. This suggests that the reference model is not an accurate model of the actual post-meningitic cochlea. A comparison between the predicted FN and ANF thresholds shows that the FN threshold is lower for all but the two most apical electrodes (1 and 2) suggesting a risk of FNS even prior to the onset of meningitis related factors. These simulations were, however, performed for the worst-case scenario of maximum FNF diameter (8 µm). Predictions of thresholds for smaller diameter FNFs would be higher and thus decrease the likelihood of FNS.

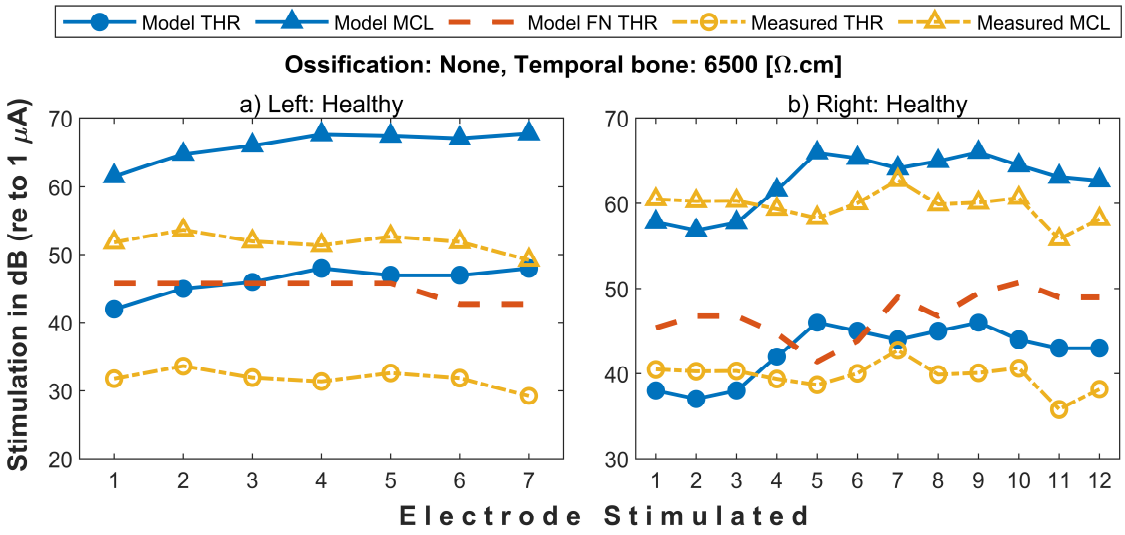

Figure 7. Predicted and measured (perceptual) thresholds and MCLs comparison for each electrode when modelled and programmed with the user's map for the *healthy, reference models*. (a) *Left ear*. The difference between the model's predicted ANF threshold and MCL levels (solid, filled marker lines) increases from approximately 10 to 18 dB as it diverges from the user's perceptual threshold and MCL data (broken, empty marker lines). This suggests that the healthy model is not an accurate model of the actual post meningitic cochlea. The predicted FN threshold (broken, unmarked line) is lower than the ANF threshold for all but the two most apical electrodes (E1 and E2) confirming possible FNS even at the lowest stimulus levels for the worst-case scenario of an 8 µm FNF diameter. (b) *Right ear*. The difference between the predicted and perceptual ANF threshold and MCL levels ranges between 5 and 10 dB, smaller compared to the left ear. E1 to E3 might be wrongly positioned within the cochlear model as their predicted thresholds are lower than the perceptual thresholds. The predicted FN thresholds are higher than most of the ANF thresholds, but the close proximity of the two threshold predictions again suggests a risk of FNS at low stimulus levels even in the absence of meningitic related factors.

Equivalent comparisons for the reference *right* cochlea in Figure 7b show predictions to be much closer to the measured, perceptual results with ANF threshold and MCL differences ranging between 5 and 10 dB. In contrast to predicted ANF thresholds almost always being higher than perceptual thresholds, the first three apical electrodes have lower predicted thresholds. This might suggest that the modelled electrode array is not positioned correctly within that section of the cochlea. Although

the FN thresholds are higher than the ANF thresholds for most electrodes, it still lies much closer to the ANF thresholds than the MCL levels which, as with the left cochlea, suggests that the user could have been at risk of FNS even without manifestation of meningitic related FNS factors.

User-specific application of the MBD tool

Predicted stimulus threshold and MCL levels versus electrode, as presented in the previous section for the reference cochleae, were repeated for the post-meningitic models using the user's map with STs and SVs ossified as described in earlier. The temporal bone resistivity was set to 5200 Ω.cm, 20% lower than normal bone, based on the May 2015 data from Figure 5 from which it was calculated that the average density for the left and the right cochleae (approximately 1890 HU) is 20% lower than the control group's average density (2207 HU). Hence, for the purpose of this study, we are assuming that the resistivity is proportional to density.

Predictions for the left ear in Figure 8a show a noticeable decrease in MCL and threshold toward the basal electrodes in contrast to an increase seen in the reference model (Figure 7a). Predicted threshold and MCL values therefore no longer diverge from the measured values' trend, but follow it more accurately. The FN thresholds show a slight and overall, almost uniform, *increase* compared to the reference model resulting in the FN threshold now being 3-8 dB *higher* than the ANF threshold where it was *lower* than the ANF threshold for the reference model. This would suggest a lowered, albeit still reasonable, risk of FNS as the FN threshold remains below the MCL.

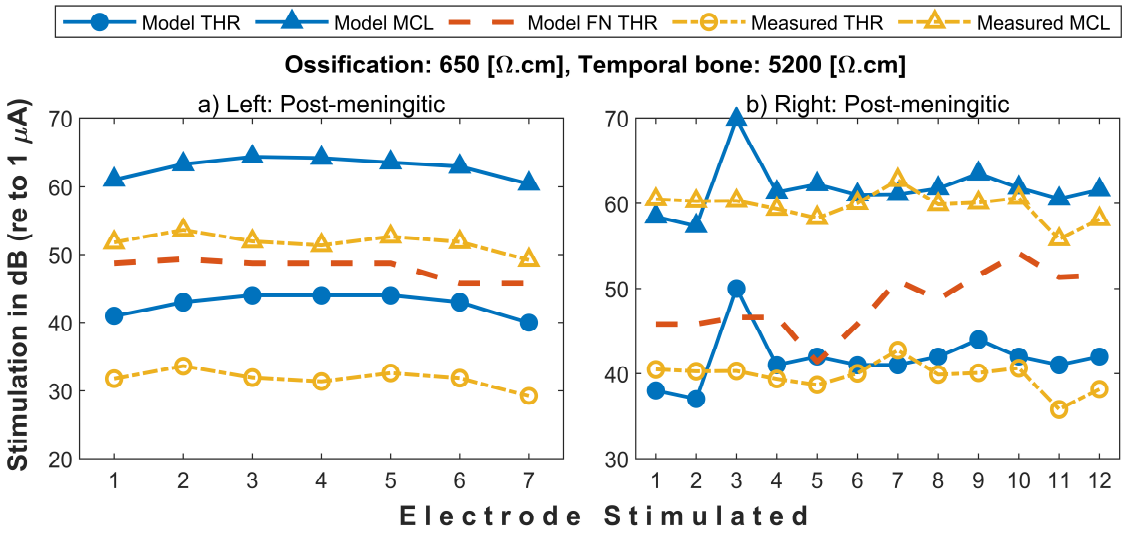

Figure 8. Predicted and measured (perceptual) thresholds and MCLs comparison for each electrode when modelled and programmed with the user's map for the *post-meningitic models*. (a) *Left ear*. Predicted thresholds no longer diverge from the measured thresholds as was the case for the healthy model (Fig 7a), but follows the perceptual trend more accurately at the basal electrodes. The FN threshold shows a slight and near-uniform increase compared to the reference model resulting in a 3 to 8 dB higher threshold than the ANF threshold. The risk of FNS, however, remains as the FN threshold remains below the MCL. (b) *Right ear*. Apart from E3, the predicted threshold and MCL levels are even closer to the perceptual values compared to the healthy model in (7b). The FN thresholds show a slight and near-uniform increase thus widening the gap between the ANF and FN thresholds as in the left cochlea.

The post-meningitic *right* cochlea's simulation results in Figure 8b show a notable resemblance between the predicted and measured threshold and MCL levels. The cause for the high threshold predicted for E3 is unsure but could be attributed to factors such as the fibres now being degenerate or incorrect electrode placement in the model. Compared to the reference model (Figure 7b), threshold and MCL levels show a small but noticeable decrease toward the perceptual levels and, as was the case for the left cochlea, the FN thresholds again show a slight and near-uniform increase. As would be expected, E5, being the electrode nearest to the FN, remains the electrode with the lowest FN threshold.

Discussion

The primary objective of this study was to apply user-specific 3D computational modelling in a translational way to create an MBD tool that allows investigation of the mechanisms that underlie the manifestation of FNS in a CI user's post-meningitic cochleae. The models were constructed based on previous work in our group (T. K. Malherbe et al., 2016) and used to assess the likelihood of FNS through the prediction of ANF and FN thresholds by including the FN and factors associated with post-meningitic cochleae into the models.

Several studies have proposed that lowered resistivity, or increased conductivity, of the otic capsule is the most probable cause of FNS as it creates possible pathways for current to leak from the cochlea to other nearby structures such as the FN (Ahn et al., 2009; Battmer et al., 2006; Cushing et al., 2006; Kelsall et al., 1997; Kruschinski et al., 2003; Makizumi et al., 2013; Marshall et al., 2005; Seyyedi et al., 2013). The bone densitometry results in Figure 5 revealed that the post-meningitic cochleae of the CI user in this study have a more severe reduction in bone resistivity than most post-otosclerotic cochleae. The effect of reduced resistivity in the otic capsule due to otosclerosis was first modelled by Frijns et al. (2009) who described the leakage current as resulting in a reduced current density in the ST and hence higher thresholds for both the ANF and FN, albeit to a lesser degree for the FN. The bone densitometry results in Figure 5 also showed a continuous decrease in the otic capsules' bone density or resistivity over time, thus suggesting an increase in FNS. This observation is supported by the changes in FNS experienced by the user and by the increase in perceptual thresholds during the same period.

After constructing user-specific models of the cochleae and including ossification within the cochlear ducts and degenerate fibres, the threshold vs. bone

resistivity graphs in Figure 6 revealed somewhat different results compared to those found in Frijns et al. (2009). The partially ossified *right* cochlea (Figure 6b) more closely resembles Frijn's healthy, non-ossified cochlear duct simulations in which the FN threshold remains "relatively constant" for higher resistivities while the ANF threshold increases more rapidly as the resistivity decreases. This convergence of the two thresholds as temporal bone resistivity decreases over time, decreases the dynamic range within which the CI can operate without causing FNS. The relatively constant FN threshold is particularly visible for E5, the electrode nearest to the FN.

In contrast to the partially ossified right cochlea, the completely ossified *left* cochlea (Figure 6a) shows a rapidly increasing threshold for both ANF and FN as the resistivity decreases below 5200 Ω.cm. It would therefore seem that ossification of the ducts, i.e. *increased* resistivity within the ducts, aggravates the impact of the *reduced* resistivity in the otic capsule. It would also appear that, in itself, ossification reduces the operable dynamic range when comparing the difference between the ANF and FN thresholds for the left and right cochleae. Despite the apical electrode (E1) of the left cochlea being further away from the FN than E1 of the right cochlea, the FN threshold is noticeably closer to the ANF threshold for the left cochlea suggesting a higher probability of FNS on the left. The same observation can be made for the two basal electrodes that are more equidistant from the FN.

The effect of ossification in the cochlear ducts, degenerate ANFs and a 20% lower temporal bone resistivity within the post-meningitic cochleae on model accuracy, was investigated using Figure 8 by comparing electrode thresholds to those of the healthy, reference cochleae in Figure 7. For both the left and right cochleae (excl. E1 – E3), the post-meningitic ANF thresholds showed a much closer correspondence to the measured, perceptual thresholds thus validating the inclusion of the three meningitic

factors to model the effect of FNS. Although the post-meningitic left cochlea's predicted ANF thresholds (Figure 8a) were not as close to the perceptual thresholds as is the case for the right cochlea (Figure 8b), they do follow the same trend as the perceptual thresholds. In contrast to the other electrodes in the right cochlea, E1 to E3's predicted ANF thresholds are *lower* than the perceptual thresholds in the reference model (Figure 7b) and E3's threshold is excessively high compared to the other electrodes in the post-meningitic model. This might suggest that these three electrodes were positioned incorrectly in the model taking into account the difficulty to accurately identify electrode locations from CTs because of the artefacts created by the metal electrodes. Other factors might include the presence of fibrous tissue encapsulating the electrode or segmental loss of the ANFs which was not included in the model.

It is known from physiological studies that electrodes close to the FN pose a higher risk of FNS (Kruschinski et al., 2003; Seyyedi et al., 2013). The post-meningitic model results of the right ear in Figure 8b showed that the FN threshold for E5, the electrode nearest the FN (see Figure 2), is the lowest of all electrodes and even slightly less than the ANF threshold which suggests a risk of FNS. Electrodes in the left cochlea are almost equidistant from the FN (Figure 2) thus resulting, as expected, in all electrodes having approximately the same predicted FN threshold (Figure 8a).

Overall, the left would appear to be more susceptible to FNS across all electrodes as the ANF and FN threshold differences are less than those on the right (except for E5 which is situated right next to the FN). This observation again corresponds to the user's experience with the left implant, which was explanted, later re-implanted with FNS re-occurring soon after and finally explanted a second and final time. This further validates the improved, post-meningitic model.

Considering the post-meningitic FN threshold curves in Figure 8a and Figure 8b, both the left and right showed a small, almost uniform increase across all electrodes compared to those of the reference models. This corresponds to the observations made for a lower temporal bone resistivity in Figure 6. In contrast to the FN thresholds, observations made in Figure 6 and in Frijns et al. (2009), the ANF thresholds *decreased* in the post-meningitic models. This could possibly be ascribed to the ossified cochlear ducts' near 10-fold increase in resistivity redirecting sufficient current through the bony spiral lamina to the degenerated ANF's axons which have lower thresholds relative to the dendrites because of their larger diameters.

Case reports such as the one presented in the present study complement evidence-based medicine as the population-based nature of large research studies often necessitate the exclusion of case-specific parameters. This approach may result in the findings from such studies to have little relevance to an individual person (Rison et al., 2017). By applying the MBD tool to assess the underlying mechanisms and the progression of FNS for the specific CI user, clinical information that is relevant for the individual could be derived. The primary implication for the user from the findings in this study is that the presentation of FNS is expected to have stabilized in the left cochlea while it is likely to deteriorate for the right cochlea as the changes in the bone in and around this cochlea are ongoing. This information may affect and ultimately determine the course of management of the specific user.

In summary, i) bone densitometry was effectively used to estimate and model the decrease in bone resistivity within the otic capsule, ii) post-meningitic predicted ANF threshold levels more closely presented the perceptual thresholds while the predicted likelihood of FNS was confirmed by the user's experience, iii) ossification of the cochlear ducts appeared to aggravate the increase in thresholds caused by the otic

capsule's decreased resistivity, iv) simulations showed good correspondence between electrode distance from the FN and its risk of causing FNS.

Finally, this translational study demonstrates the value of computational modelling as a clinical instrument in the assessment and management of complications with CI implantation.

Acknowledgements

The authors wish to thank and acknowledge Dr Maurice Hockmann and Ms Wendy Deverson for support and discussions of the specific case as well as the user for agreeing to participate in the study.

References

Ahn, J. H., Oh, S. H., Chung, J. W., & Lee, K. S. (2009). Facial nerve stimulation after cochlear implantation according to types of Nucleus 24-channel electrode arrays. *Acta Otolaryngol*, *129*(6), 588-591. https://doi.org/10.1080/00016480802325965

Akst, L. M., & Weber, P. C. (2005). Facial nerve management in cochlear implant surgery. *Operative Techniques in Otolaryngology-Head and Neck Surgery*, *16*(2), 78-81. https://doi.org/10.1016/j.otot.2005.05.013

Axon, P. R., Temple, R. H., Saeed, S. R., & Ramsden, R. T. (1998). Cochlear ossification after meningitis. *Am J Otol*, *19*(6), 724-729. https://www.ncbi.nlm.nih.gov/pubmed/9831144

Badenhorst, W., Hanekom, T., & Hanekom, J. J. (2017). Analysis of a purely conductance-based stochastic nerve fibre model as applied to compound models of populations of human auditory nerve fibres used in cochlear implant simulations [journal article]. *Biol Cybern*, *111*(5-6), 439-458. https://doi.org/10.1007/s00422-017-0736-8

Balmer, T. W., Vesztergom, S., Broekmann, P., Stahel, A., & Büchler, P. (2018). Characterization of the electrical conductivity of bone and its correlation to osseous structure. *Sci Rep*, *8*(1), 8601. https://doi.org/10.1038/s41598-018-26836-0

Battmer, R., Pesch, J., Stover, T., Lesinski-Schiedat, A., Lenarz, M., & Lenarz, T. (2006). Elimination of facial nerve stimulation by reimplantation in cochlear implant subjects. *Otol Neurotol*, *27*(7), 918-922. https://doi.org/10.1097/01.mao.0000235374.85739.c6

Berrettini, S., Vito de, A., Bruschini, L., Passetti, S., & Forli, F. (2011). Facial nerve stimulation after cochlear implantation: our experience. *Acta otorhinolaryngologica Italica : organo ufficiale della Societa italiana di*

otorinolaringologia e chirurgia cervico-facciale, *31*(1), 11-16. https://www.ncbi.nlm.nih.gov/pubmed/21808458

Bigelow, D. C., Kay, D. J., Rafter, K. O., Montes, M., Knox, G. W., & Yousem, D. M. (1998). Facial nerve stimulation from cochlear implants. *Am J Otol*, *19*(2), 163-169. https://www.ncbi.nlm.nih.gov/pubmed/9520052

Bille, J., & Ovesen, T. (2014). Cochlear implant after bacterial meningitis. *Pediatr Int*, *56*(3), 400-405. https://doi.org/10.1111/ped.12252

Briaire, J. J., & Frijns, J. H. (2006). The consequences of neural degeneration regarding optimal cochlear implant position in scala tympani: a model approach. *Hear Res*, *214*(1-2), 17-27. https://doi.org/10.1016/j.heares.2006.01.015

Caye-Thomasen, P., Dam, M. S., Omland, S. H., & Mantoni, M. (2012). Cochlear ossification in patients with profound hearing loss following bacterial meningitis. *Acta Otolaryngol*, *132*(7), 720-725. https://doi.org/10.3109/00016489.2012.656323

Cushing, S. L., Papsin, B. C., & Gordon, K. A. (2006). Incidence and characteristics of facial nerve stimulation in children with cochlear implants. *Laryngoscope*, *116*(10), 1787-1791. https://doi.org/10.1097/01.mlg.0000231303.85828.20

Du, Y., Wu, X., & Li, L. (2006). Mechanisms of bacterial meningitis-related deafness. *Drug Discovery Today: Disease Mechanisms*, *3*(1), 115-118. https://doi.org/10.1016/j.ddmec.2006.02.002

Durisin, M., Bartling, S., Arnoldner, C., Ende, M., Prokein, J., Lesinski-Schiedat, A., Lanfermann, H., Lenarz, T., & Stover, T. (2010). Cochlear osteoneogenesis after meningitis in cochlear implant patients: a retrospective analysis. *Otol Neurotol*, *31*(7), 1072-1078. https://doi.org/10.1097/mao.0b013e3181e71310

Eshraghi, A. A., Telischi, F. F., Hodges, A. V., Odabasi, O., & Balkany, T. J. (2004). Changes in programming over time in postmeningitis cochlear implant users. *Otolaryngol Head Neck Surg*, *131*(6), 885-889. https://doi.org/10.1016/j.otohns.2004.05.019

Farinetti, A., Ben Gharbia, D., Mancini, J., Roman, S., Nicollas, R., & Triglia, J. M. (2014). Cochlear implant complications in 403 patients: comparative study of adults and children and review of the literature. *Eur Ann Otorhinolaryngol Head Neck Dis*, *131*(3), 177-182. https://doi.org/10.1016/j.anorl.2013.05.005

Fatterpekar, G. M., Doshi, A. H., Dugar, M., Delman, B. N., Naidich, T. P., & Som, P. M. (2006). Role of 3D CT in the evaluation of the temporal bone. *Radiographics*, *26 Suppl 1*, S117-132. https://doi.org/10.1148/rg.26si065502

Felder, E., Kanonier, G., Scholtz, A., Rask-Andersen, H., & A Schrott-Fischer, A. (1997). Quantitative evaluation of cochlear neuronal and computer-aided three-dimensional reconstruction of spiral ganglion cells in humans with a peripheral loss of nerve fibres. *Hearing Research*, *105*(1-2), 183-190. http://www.scopus.com/inward/record.url?eid=2-s2.0-0031106657&partnerID=40&md5=e0b18cd749433c7dbcb7c8b639afea96

Frijns, J. H., Kalkman, R. K., & Briaire, J. J. (2009). Stimulation of the facial nerve by intracochlear electrodes in otosclerosis: a computer modeling study. *Otol Neurotol*, *30*(8), 1168-1174. https://doi.org/10.1097/MAO.0b013e3181b12115

Grayeli, A. B., Yrieix, C. S., Imauchi, Y., Cyna-Gorse, F., Ferrary, E., & Sterkers, O. (2004). Temporal bone density measurements using CT in otosclerosis. *Acta Otolaryngol*, *124*(10), 1136-1140. https://doi.org/10.1080/00016480410018188

Hanekom, T. (2005). Modelling encapsulation tissue around cochlear implant electrodes. *Med Biol Eng Comput*, *43*(1), 47-55. https://doi.org/10.1007/bf02345122

Hanekom, T., & Hanekom, J. J. (2016). Three-dimensional models of cochlear implants: A review of their development and how they could support management and maintenance of cochlear implant performance [Article in Press]. *Network*, *27*(2-3), 67-106. https://doi.org/10.3109/0954898X.2016.1171411

Johnson, M. H., Hasenstab, M. S., Seicshnaydre, M. A., & Williams, G. H. (1995). CT of Postmeningetic Deafness: Observations and Predictive Value for Cochlear Implants in Children. *AMJ Neuroradiol*, *16*, 103-109.

Kalkman, R. K., Briaire, J. J., & Frijns, J. H. (2016). Stimulation strategies and electrode design in computational models of the electrically stimulated cochlea: An overview of existing literature [Article in Press]. *Network*, *27*(2-3), 107-134. https://doi.org/10.3109/0954898X.2016.1171412

Kawase, S., Naganawa, S., Sone, M., Ikeda, M., & Ishigaki, T. (2006). Relationship between CT densitometry with a slice thickness of 0.5 mm and audiometry in otosclerosis. *Eur Radiol*, *16*(6), 1367-1373. https://doi.org/10.1007/s00330-005-0128-7

Kelsall, D. C., Shallop, J. K., Brammeier, T. G., & Prenger, E. C. (1997). Facial nerve stimulation after Nucleus 22-channel cochlear implantation. *Am J Otol*, *18*(3), 336-341. https://www.ncbi.nlm.nih.gov/pubmed/9149828

Klein, M., Koedel, U., Kastenbauer, S., & Pfister, H. W. (2008). Nitrogen and oxygen molecules in meningitis-associated labyrinthitis and hearing impairment. *Infection*, *36*(1), 2-14. https://doi.org/10.1007/s15010-007-7153-1

Kruschinski, C., Weber, B. P., & Pabst, R. (2003). Clinical relevance of the distance between the cochlea and the facial nerve in cochlear implantation. *Otol Neurotol*, *24*(5), 823-827. https://doi.org/10.1097/00129492-200309000-00022

Kutlar, G., Koyuncu, M., Elmali, M., Basar, F., & Atmaca, S. (2014). Are computed tomography and densitometric measurements useful in otosclerosis with mixed hearing loss? A retrospective clinical study. *Eur Arch Otorhinolaryngol*, *271*(9), 2421-2425. https://doi.org/10.1007/s00405-013-2729-0

Makizumi, Y., Kashio, A., Sakamoto, T., Karino, S., Kakigi, A., Iwasaki, S., & Yamasoba, T. (2013). Cochlear implantation in a patient with osteogenesis imperfecta. *Auris Nasus Larynx*, *40*(5), 510-513. https://doi.org/10.1016/j.anl.2012.10.006

Malherbe, T. K., Hanekom, T., & Hanekom, J. J. (2013). Can subject-specific single-fibre electrically evoked auditory brainstem response data be predicted from a model? *Medical Engineering & Physics*, *35*(7), 926-936. https://doi.org/10.1016/j.medengphy.2012.09.001

Malherbe, T. K., Hanekom, T., & Hanekom, J. J. (2015). The effect of the resistive properties of bone on neural excitation and electric fields in cochlear implant models. *Hear Res*, *327*, 126-135. https://doi.org/10.1016/j.heares.2015.06.003

Malherbe, T. K., Hanekom, T., & Hanekom, J. J. (2016). Constructing a three-dimensional electrical model of a living cochlear implant user's cochlea. *Int J Numer Method Biomed Eng*, *32*(7). https://doi.org/10.1002/cnm.2751

Marshall, A. H., Fanning, N., Symons, S., Shipp, D., Chen, J. M., & Nedzelski, J. M. (2005). Cochlear implantation in cochlear otosclerosis. *Laryngoscope*, *115*(10), 1728-1733. https://doi.org/10.1097/01.mlg.0000171052.34196.ef

Maru, N., Cheita, A. C., Mogoanta, C. A., & Prejoianu, B. (2010). Intratemporal course of the facial nerve: morphological, topographic and morphometric features. *Rom J Morphol Embryol*, *51*(2), 243-248. https://www.ncbi.nlm.nih.gov/pubmed/20495738

Nadol, J. B. (1990). Degeneration of Cochlear Neurons as Seen in the Spiral Ganglion of Man. *Hearing Research*, *49*(1-3), 141-154. https://doi.org/Doi 10.1016/0378-5955(90)90101-T

Nadol, J. B., Jr., Young, Y. S., & Glynn, R. J. (1989). Survival of spiral ganglion cells in profound sensorineural hearing loss: implications for cochlear implantation [Article]. *Ann Otol Rhinol Laryngol*, *98*(6), 411-416. https://doi.org/10.1177/000348948909800602

Niparko, J. K., Oviatt, D. L., Coker, N. J., Sutton, L., Waltzman, S. B., & Cohen, N. L. (1991). Facial nerve stimulation with cochlear implantation. VA Cooperative Study Group on Cochlear Implantation. *Otolaryngol Head Neck Surg*, *104*(6), 826-830. https://doi.org/10.1177/019459989110400610

Pfingst, B. E., Bowling, S. A., Colesa, D. J., Garadat, S. N., Raphael, Y., Shibata, S. B., Strahl, S. B., Su, G. L., & Zhou, N. (2011). Cochlear infrastructure for electrical hearing. *Hear Res*, *281*(1-2), 65-73. https://doi.org/10.1016/j.heares.2011.05.002

Pfingst, B. E., Zhou, N., Colesa, D. J., Watts, M. M., Strahl, S. B., Garadat, S. N., Schvartz-Leyzac, K. C., Budenz, C. L., Raphael, Y., & Zwolan, T. A. (2015). Importance of cochlear health for implant function [Review]. *Hear Res*, *322*, 77-88. https://doi.org/10.1016/j.heares.2014.09.009

Phillips, C. D., & Bubash, L. A. (2002). The facial nerve: anatomy and common pathology. *Semin Ultrasound CT MR*, *23*(3), 202-217. https://doi.org/10.1016/s0887-2171(02)90047-8

Postelmans, J. T., Cleffken, B., & Stokroos, R. J. (2007). Post-operative complications of cochlear implantation in adults and children: five years' experience in Maastricht. *J Laryngol Otol*, *121*(4), 318-323. https://doi.org/10.1017/S0022215106003471

Rattay, F., Lutter, P., & Felix, H. (2001). A model of the electrically excited human cochlear neuron. I. Contribution of neural substructures to the generation and propagation of spikes. *Hear Res*, *153*(1-2), 43-63. https://doi.org/10.1016/s0378-5955(00)00256-2

Rauch, S. D., Herrmann, B. S., Davis, L. A., & Nadol, J. B., Jr. (1997). Nucleus 22 cochlear implantation results in postmeningitic deafness. *Laryngoscope*, *107*(12 Pt 1), 1606-1609. https://doi.org/10.1097/00005537-199712000-00005

Rison, R. A., Shepphird, J. K., & Kidd, M. R. (2017). How to choose the best journal for your case report. *Journal of Medical Case Reports*, *11*(1), 198. https://doi.org/10.1186/s13256-017-1351-y

Rotteveel, L. J., Proops, D. W., Ramsden, R. T., Saeed, S. R., van Olphen, A. F., & Mylanus, E. A. (2004). Cochlear implantation in 53 patients with otosclerosis: demographics, computed tomographic scanning, surgery, and complications. *Otol Neurotol*, *25*(6), 943-952. https://doi.org/10.1097/00129492-200411000-00014

Saha, S., & Williams, P. A. (1989). Electric and dielectric properties of wet human cancellous bone as a function of frequency. *Ann Biomed Eng*, *17*(2), 143-158. https://doi.org/10.1007/bf02368024

Şentürk, M., Somdas, M., Ekinci, N., Bayram, A., Erkorkmaz, Ü., & Ünlü, Y. (2009). Important landmarks for facial canal in the middle ear and mastoid: Human cadaveric temporal bone study. *Erciyes Tip Dergisi*, *31*, 201-207.

Seyyedi, M., Herrmann, B. S., Eddington, D. K., & Nadol, J. B., Jr. (2013). The pathologic basis of facial nerve stimulation in otosclerosis and multi-channel cochlear implantation. *Otol Neurotol*, *34*(9), 1603-1609. https://doi.org/10.1097/MAO.0b013e3182979398

Shin, K. J., Gil, Y. C., Lee, J. Y., Kim, J. N., Song, W. C., & Koh, K. S. (2014). Three-dimensional study of the facial canal using microcomputed tomography for improved anatomical comprehension. *Anat Rec (Hoboken)*, *297*(10), 1808-1816. https://doi.org/10.1002/ar.22977

Thurner, K. H., Egg, G., Spoendlin, H., & Schrott-Fischer, A. (1993). A quantitative study of nerve fibers in the human facial nerve. *Eur Arch Otorhinolaryngol*, *250*(3), 161-167. https://doi.org/10.1007/bf00171704

Tinling, S. P., Colton, J., & Brodie, H. A. (2004). Location and timing of initial osteoid deposition in postmeningitic labyrinthitis ossificans determined by multiple fluorescent labels. *Laryngoscope*, *114*(4), 675-680. https://doi.org/10.1097/00005537-200404000-00015

Verbist, B. M., Skinner, M. W., Cohen, L. T., Leake, P. A., James, C., Boex, C., Holden, T. A., Finley, C. C., Roland, P. S., Roland, J. T., Jr., Haller, M., Patrick, J. F., Jolly, C. N., Faltys, M. A., Briaire, J. J., & Frijns, J. H. (2010). Consensus panel on a cochlear coordinate system applicable in histologic, physiologic, and radiologic studies of the human cochlea. *Otol Neurotol*, *31*(5), 722-730. https://doi.org/10.1097/MAO.0b013e3181d279e0